WIRELESS BATTERY CHARGE MANAGEMENT FOR IMPLANTABLE PRESSURE SENSOR

Steve Majerus[1,2], Steven L. Garverick[2], and Margot S. Damaser[1,3]

[1]Advanced Platform Technology Center
Louis Stokes Cleveland VA Medical Center
Cleveland, OH

[2]Dept. of Electrical Engineering and Computer Science
Case Western Reserve University
Cleveland, OH

[3]Dept. of Biomedical Engineering
Cleveland Clinic
Cleveland, OH

***Abstract*-Implantable medical devices intended for chronic application in deep bodily organs must balance small size with battery capacity. Wireless battery recharge of implanted sensors is a viable option to reduce implant size while removing the physical and regulatory hindrance of continuous RF powering. This paper presents wireless battery recharge circuitry developed for an implantable pressure sensor. The circuits include an RF/DC rectifier, voltage limiter, and constant-current battery charger with 150-mV end-of-charge hysteresis. An AM demodulator drawing zero DC current allows for transmission of commands on the recharge carrier. Reception of a time- and value-coded shutdown command places the implantable system into a 15-nano-Ampere standby mode. The system can be wirelessly activated from standby by reactivating the external wireless recharge carrier. Test results of the wireless system showed a standby current of 15-nA, such that the implant standby time is limited by battery self-discharge. Wireless recharge tests confirmed that a constant recharge rate of 200 µA could be sustained at implant depths up to 20 cm, but with low power transfer efficiency < 0.1% due to small implant coil size. Battery charge measurements confirmed that daily 4-hour recharge periods maintained the implant state of charge and this recharging could occur during periods of natural patient rest.**

I. INTRODUCTION

Chronic bladder pressure monitoring is required in urodynamics to diagnose disease and to facilitate neuromodulation for bladder control and rehabilitation. Existing implantable bladder pressure sensors have generally targeted acute applications, and have not been designed for permanent fixation within the bladder. Moreover, several existing bladder pressure sensors [1] - [2] use primary cell batteries and transmit pressure data at millihertz rates to save energy; this data rate is too sparse to record bladder contractions well enough for urodynamics or neuromodulation.

We have developed an implantable pressure sensor called the wireless implantable micro-manometer (WIMM) designed specifically for chronic bladder pressure monitoring [3] - [4]. One key feature that enables chronic application of the WIMM is its long-range, wireless battery recharge capability, which can maintain the battery state of charge through daily wireless recharge sessions. An illustration of the WIMM concept is shown in Fig. 1, indicating that the implanted sensor is wirelessly recharged by externally-applied RF power.

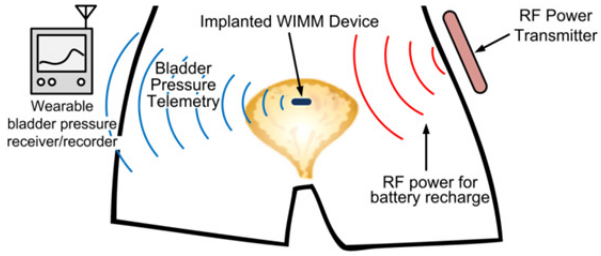

Fig. 1. Illustration of WIMM system concept. The WIMM is implanted within the bladder wall and transmits telemetry to an external receiver. Intermittent RF recharge is used to maintain the battery charge.

II. WIRELESS BATTERY RECHARGER AND POWER STANDBY COMMAND RECEIVER

Chronically-implanted systems deep within the abdominal cavity must be small to prevent erosion, migration, or other complications. Furthermore, the distance from the implanted device to an external transceiver can be 20 cm or greater in obese patients. Size-constrained RF-powered sensors have very low efficiency at this distance [5] and passive sensors such as [6] are mainly suitable for shallow implantation depths. Instead of continuous RF powering, the WIMM runs primarily from a micro-battery and RF-recharge would occur during 6-hour periods, e.g. when the user is sleeping.

The implantable WIMM sensor consists of a mixed-signal ASIC, MEMS pressure sensor, rechargeable battery, and antennas for data transmission and RF battery recharge. All of the active circuitry for instrumentation, telemetry, and power management is integrated on the ASIC (Fig. 2a). The size of the assembled device is shown in the photograph of Fig. 2b, and it is evident that the rechargeable battery and wireless recharge coil occupy about half of the implant volume.

The battery size was chosen to provide adequate capacity for over 24 hours of implant operation based on the average active current draw [7]. Optimization of the wireless recharge coil geometry was performed, and a 30-turn, 11-µH coil was designed to fit around the implant components. Ferrite rods were added to increase the coil inductance, and a wireless recharge frequency of 3 MHz was selected as reported in [8].

While this previous work determined an optimal recharge frequency based on approximate device size and implant distance for the proposed microsystem, the circuitry described

978-1-4799-5924-2/14/$31.00 ©2014 IEEE

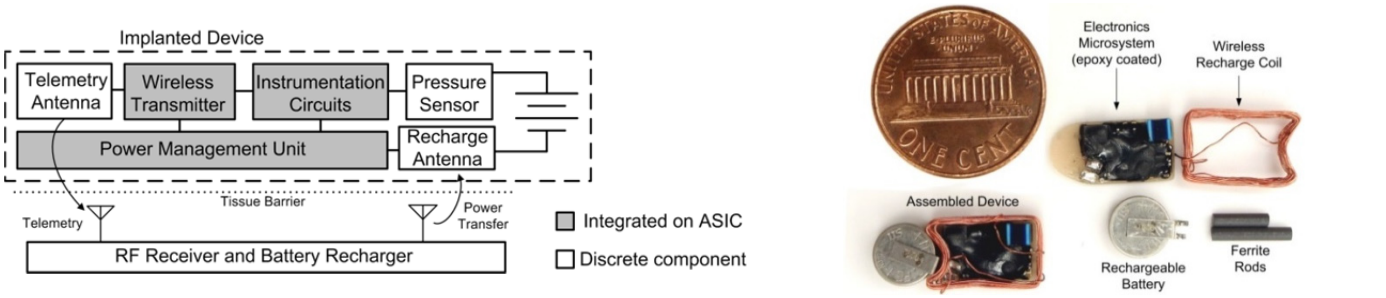

Fig. 2. Schematic views of the proposed WIMM: (a) system block diagram consisting of implanted device and external RF receiver and battery recharger and (b) components within the WIMM include custom electronics, rechargeable battery, ferrite rods, and a wound coil for wireless battery recharge.

here was integrated with the telemetry ASIC and includes a low-overhead capability for wirelessly-commanded device standby. Further optimization of the external recharging antenna, as well as a new geometry for the implanted power receiving coil permit long-distance wireless recharge of the implanted battery at double the rate reported in [8].

A. RF/DC Rectifier and Battery Charger

The wireless battery recharging circuitry on the ASIC is organized into three sections: an RF/DC rectifier, passive voltage limiter, and a constant-current battery charger. All circuits draw power from the rectified RF voltage captured by the recharge coil, RFV_{DD}, and a schematic for the RF/DC battery charger is shown in Fig. 3. Inductor L_1 represents the wireless recharge coil and C_1 is used to tune the tank circuit to resonate at 3 MHz.

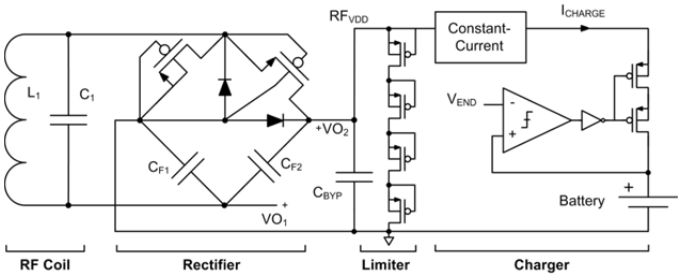

Fig. 3. The wireless battery recharge circuitry integrated on the ASIC consists of a passive voltage doubler rectifier to extract DC power from the RF pickup coil. A voltage limiter protects the circuitry from excess voltage and a constant-current charger maintains the battery charge up to voltage V_{END}.

The RF/DC rectifier topology used on the ASIC is a simple, passive voltage doubler circuit [9]. This circuit was chosen over more complex, active rectifiers for its simplicity, compact size, and ability to produce two output voltages, VO_1 and VO_2. The main drawback of the circuit is that capacitors $C_{F1,2}$ are too large to be integrated on chip, and the approximate capacitor size for C_{F2} was calculated based on tolerable ripple voltage V_{r2} and by assuming that the current drawn from VO_2 was much larger than that drawn from VO_1 as

$$V_{r2} = \frac{I_{O2}}{C_{F2} f} \quad (1)$$

where f is the RF energy frequency. For a 3-MHz recharge frequency and 200 μA battery recharge current, C_{F2} was chosen as 1 nF to limit the rectified ripple to about 70 mV. Regulation of the rectified RFV_{DD} level is not needed for battery recharge, but protection of the charging circuitry is needed to prevent battery and/or circuit damage if an excessive level of RF energy is captured. A passive voltage limiter consisting of a stack of diode-connected PMOS transistors functions as a shunt regulator and effectively limits RFV_{DD} to about 5 V.

The battery recharge circuit was designed to recharge lithium-ion coin cells, e.g. the Seiko MS621FE [10] used by the implantable microsystem. Typically, lithium-ion cells are recharged with a constant-current and a constant-voltage phase but to simplify the circuitry and to prevent battery overvoltage, the ASIC battery charger only uses a constant-current phase to charge the battery to about 90% of its total capacity. A constant recharge current of 200 μA is applied to the battery whenever the voltage is below V_{END}. A comparator with 150 mV hysteresis detects if the battery voltage exceeds V_{END} and prevents battery overcharge.

B. Nano-amp Wireless Standby and Wake Receiver

In the standby mode, power to the analog portions of the ASIC is disabled, while the digital circuits remain powered, but unclocked to preserve the state of the standby control memory. The standby command is transmitted as 20% AM modulation on the battery recharge field, and a time-based command decoder verifies that the command signal timing is correct before entering standby. The ASIC exits standby after the wireless recharge field is re-applied.

The AM demodulation circuit and command decoder is illustrated in Fig. 4, and all components are integrated monolithically. The RF input is taken from the wireless recharging coil, and the carrier is filtered out by $R_{1,2}$ and C_1. The resistors divide the signal by 3 and limit the recharge coil loading while $M_{1,2}$ limit V_X to about -0.5 – RFV_{DD}, where RFV_{DD} is the RF/DC rectifier output. During recharge, V_X is equal to 1.7 V with a small 3-MHz ripple. Schmitt trigger inverters convert the voltage at V_X to a binary signal which drives a T-flip-flop. When the RF recharge signal drops suddenly, i.e. during AM modulation, the output state of the T-flip-flop toggles. The command decoder interprets the digital signal to determine if a true standby command was sent.

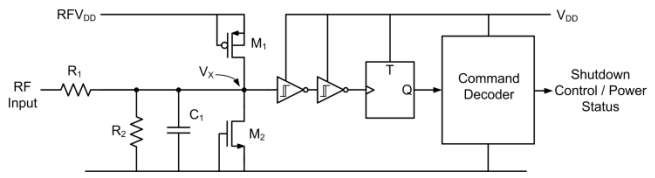

Fig. 4. Battery recharge envelope demodulator and command decoder. This circuit draws no DC current from the recharger supply, RFV_{DD} and can demodulate and decode commands transmitted in the recharge carrier envelope.

Because the standby command is used infrequently, the command decoder timing was designed to be robust and convoluted to prevent accidental ASIC shutdown due to RF interference. The decoder only places the ASIC into standby when a command matches both a time- and value-based check, as described in Fig. 5. The decoder must receive exactly 3 negative edges within 10 ms, and this pattern must be repeated for 6 successive 40-ms periods to enable the shutdown output. If the decoder input pattern fails the checking process, the decoder is "locked" for 20 ms and ignores further modulation attempts. In standby mode the command decoder clock source is disabled, so the circuit is entirely edge-triggered. The command decoder releases the ASIC from standby when wireless battery recharge is reactivated.

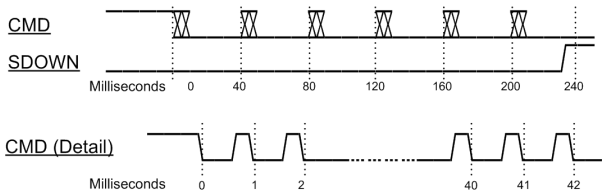

Fig. 5. Timing diagram for the command decoder that puts the ASIC in standby. A certain pattern of bits must be received within a time window to avoid accidental shutdown of the ASIC.

Power control for the ASIC during standby is depicted in Fig. 6, where AV_{DD} and DV_{DD} are the analog and digital voltage supplies, respectively. The PWREN signal from the command decoder controls whether the implant is running or in standby. Normally, AV_{DD} is coupled to analog and digital supply lines but when standby is entered, DV_{DD} is first shorted to the battery voltage before being disconnected from the regulator to ensure that the digital circuits remain powered throughout the supply changeover to prevent loss of the latched standby command. The length of the supply changeover overlap is determined by the propagation delay of a chain of long inverters; a delay of 500 ns was used to allow for sufficient turn-on time for the power gating FETs.

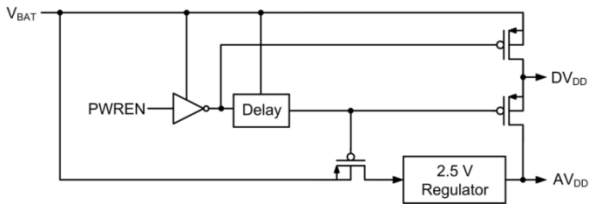

Fig. 6. The main power control circuit controlled by input signal PWREN. When PWREN is low the ASIC enters standby mode in a controlled manner to avoid power supply interruptions to the digital logic.

III. Wireless Battery Charger and Standby Receiver Test Results

Wireless recharge testing of the system was performed by coupling voltage sense leads to the microsystem battery. A class-E amplifier operating at 3 MHz provided energy to the microsystem through a 6-turn, 12-cm diameter, 12-µH coil antenna. The amplifier output power was varied such that the minimum power to sustain a 200-µA recharge current was delivered to the microsystem for a given separation distance between transmitting antenna and wireless implant. Unless otherwise noted, presented results were measured at a separation distance of 20 cm and an amplifier output power of 21 W.

An example 48-hour charge/discharge curve for the wireless microsystem is shown in Fig. 7. The wireless charging circuit fully charged the battery in about 4 hours, and limited the battery voltage to 3.45 V. After the wirelessly-transmitted recharge field was shut off, the microsystem functioned for 24 hours while continuously transmitting pressure data at 100 Hz, showing that daily recharge sessions are sufficient to maintain battery charge of the implanted pressure sensor.

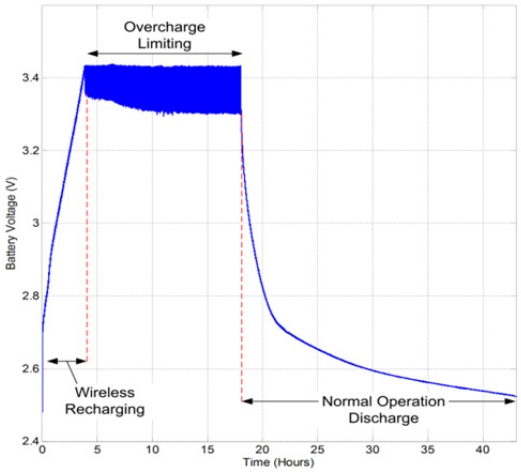

Fig. 7. Measured battery voltage during wireless recharge and normal operation. A voltage limiter stops recharge once the battery reaches a fixed threshold, and a 4 hour daily recharge is sufficient for chronic use.

One parameter for a chronically-implanted device is the implant depth because wireless recharge must be feasible at potentially large distances. Previous studies of the microsystem demonstrated recharging at depths of 10 cm with a maximum of 30° coaxial coil misalignment [8]. However, as the WIMM was miniaturized, the power transfer efficiency (η) to the device was reduced. The power required to recharge the battery at a rate of 200 µA was measured at various distances from the transmitting coil, as displayed in Fig. 8. Generally, the power transfer efficiency is well below 1%, but wireless recharge at implantation depths of 20 cm is still possible. Note that the measured power transfer was at the 200-µA recharge rate; longer charge times at a lower rate would be achievable with a reduced level of externally-transmitted energy.

Although the measured power transfer efficiency is quite

low, it roughly matches calculated wireless link efficiency η,

$$\eta = \frac{k^2 Q_1 Q_2}{\left(1+\sqrt{1+k^2 Q_1 Q_2}\right)^2}, \qquad (2)$$

where $Q_{1,2}$ are the quality factors of the external and implanted coils and k is the coupling coefficient between the coils [6]. Higher power transfer efficiency at short distances could be achieved with a small external coil but k would drop off faster with distance. The size of the external coil was thus chosen to provide reasonable η at separation distances greater than 10 cm as in normal implantation within the human bladder.

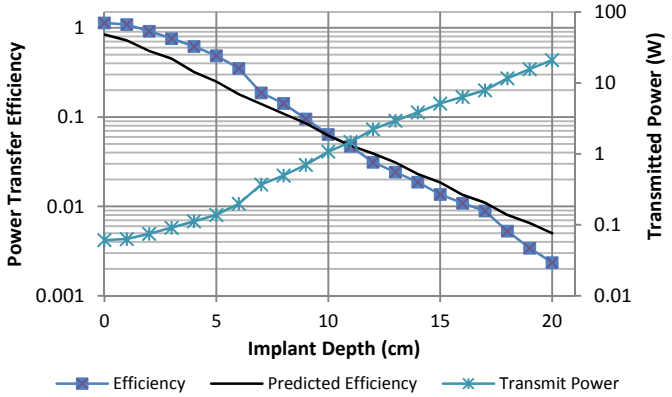

Fig. 8. Measured and predicted wireless power transfer efficiency versus device implant depth with transmitted power on secondary axis. Implantation to 20 cm is feasible with moderate levels of externally-transmitted power.

The functionality of the wirelessly-commanded standby function was also tested during RF recharge. First, the demodulator circuit from Fig. 4 was tested by applying 20% amplitude modulation to the RF recharge carrier. The demodulator output toggled at ½ the modulation rate, as expected due to the T-flip-flop memory element, as depicted in Fig. 9.

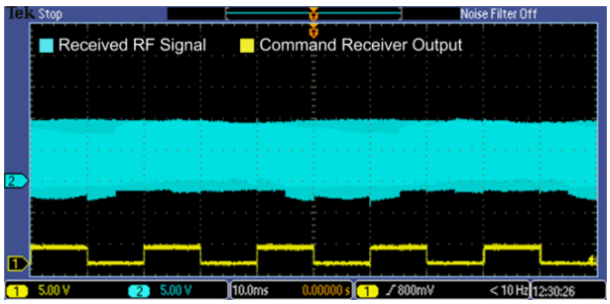

Fig. 9. Example command demodulation from 3-MHz recharge carrier. The shutdown command places the implant into a 15-nA standby mode.

To characterize the standby performance, a precision ammeter (Keithley 6482) was connected in series with the implant battery. After the implant was running, the wireless standby command was transmitted to the device by modulating the RF recharge carrier as previously described. When the device entered standby, the total battery current dropped to 15 nA within about 30 seconds. After a period of standby, the RF recharge field was reactivated, and normal implant operation resumed. An oscilloscope trace demonstrating the standby/wakeup sequence is shown in Fig. 10.

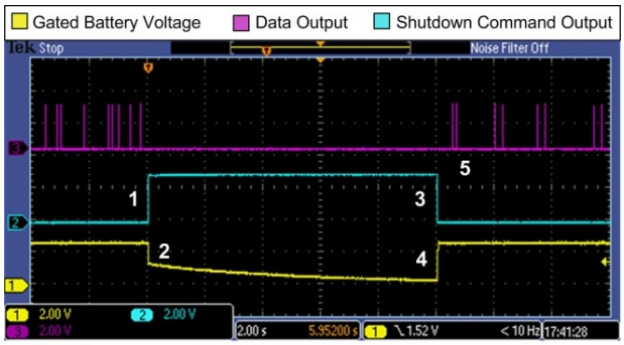

1. Standby command received
2. Implant enters nA standby mode
3. Wakeup command received
4. Implant leaves standby mode
5. Implant resumes data transmission

Fig. 10. Oscilloscope trace showing (top to bottom) WIMM data output, standby decoder output, and battery current. After the standby command is received, a 15-nA standby mode is entered. When the device is reactivated 30 seconds later, normal pressure data transmission resumes.

At the measured 15-nA level of standby current, the implant battery charge state is limited by the self-discharge characteristics of the battery, and the predicted standby time for the implant exceeds one year.

IV. Conclusion

Implanted medical devices with rechargeable batteries must account for battery charge management, and RF charging via inductive link can support devices implanted deep within the body. Here we presented a set of simple integrated circuits for wireless battery recharge and wirelessly-commanded device standby mode. Measured results confirmed that a wireless recharge rate of 200 µA could be maintained at implant depths up to 20 cm, and the device standby current of 15 nA is below the self-discharge rate of the implanted battery, allowing for very long standby periods with little loss of battery charge.

VI. References

[1] F. Axisa et al. "Design and fabrication of a low cost impantable bladder pressure monitor," in *Intl. Conf. of the IEEE Engineering in Medicine and Biology Society (EMBC)*, 2009.

[2] C. Wang et al. "A mini-invasive long-term bladder urine pressure measurement ASIC and system," *IEEE Transactions on Biomedical Circuits and Systems,* vol. 2, no. 1, pp. 44-49, 2008.

[3] S. Majerus et al. "Low-power wireless micromanometer system for acute and chronic bladder-pressure monitoring," *IEEE Transactions on Biomedical Engineering,* vol. 58, no. 3, pp. 763-768, 2011.

[4] S. Majerus et al. "Wireless, ultra-low-power implantable sensor for chronic bladder pressure monitoring," *ACM Journal of Emerging Technology,* vol. 8, no. 2, pp. 11.1-11.13, 2012..

[5] R.-F. Xue et al. "High-Efficiency Wireless Power Transfer for Biomedical Implants by Optimal Resonant Load Transformation," *IEEE Trans. on Circuits and Systems I,* vol. 60, no. 4, pp. 867-874, 2012.

[6] N. Xue, S. Chang and J. Lee, "A SU-8-based microfabricated implantable inductively coupled passive RF wireless intraocular pressure sensor," in *, 2011 Annual International Conference of the IEEE Engineering in Medicine and Biology Society (EMBC)*, 2011.

[7] S. Majerus and S. Garverick, "Power management circuits for a 15-µA, implantable pressure sensor," in *2013 IEEE Custom Integrated Circuits Conference (CICC)*, pp. 22-25, Sept. 2013.

[8] P. Cong, M. A. Suster, N. Chaimanonart and D. J. Young, "Wireless Power Recharging for Implantable Bladder Pressure Sensor," in *IEEE Sensors 2009*, Christchurch, 2009.

[9] P. Cong et al. "A wireless and batteryless 10-bit implantable blood pressure sensing microsystem with adaptive RF powering for real-time laboratory mice monitoring," *IEEE Journal of Solid-State Circuits,* vol. 44, no. 12, pp. 3631-3644, 2009.

[10] Seiko Instruments, Inc., "Micro Battery Product Catalogue," 2014. Available: http://www.sii.co.jp/en/me/files/2014/03/battery_en.pdf.